Morphological Function of Trace Fossil Paleodictyon: an Approach from Fluid Simulation

AUTHOR(S):

Kikuchi, Kazuki; Naruse, Hajime

Paleontological Research, vol. 26, no. 4, pp. 378–389, October 1, 2022

doi:10.2517/PR210001

Morphological function of trace fossil *Paleodictyon*: An approach from fluid simulation

KAZUKI KIKUCHI AND HAJIME NARUSE

Department of Geology and Mineralogy, Graduate School of Science, Kyoto University, Kitashirakawaoiwake-cho, Sakyo-ku, Kyoto 606-8502, Japan (e-mail: kikuchi@kueps.kyoto-u.ac.jp)

Received January 10, 2021; Revised manuscript accepted May 16, 2021; Published online August 1, 2022

Abstract. **This study examined the functional morphology of the trace fossil *Paleodictyon* in terms of computational fluid dynamics. The modern specimens show a unique morphology that is composed of a hexagonal mesh structure, vertical shafts opening to the seafloor, and a shield-like mound on the seafloor. The traces of the vertical shafts were also preserved in some fossil examples. To explain their characteristic morphology, a "passive ventilation" hypothesis has been proposed suggesting that their function was to ventilate their burrows with bottom currents, which supply both oxygenated water and food. However, this hypothesis has not yet been verified. This study conducted numerical experiments to understand the functions of the structures created by this ichnofossil by using a model of computational fluid dynamics with the 3D geometry of *Paleodictyon* and estimating the efficiency of the ventilation in burrows. As a result, it was observed that seawater flowed in the vertical shafts in the marginal area of the mound, and flowed out from the shafts located on the top of the mound, flowing through the mesh structure. This ventilation was observed only in the case that *Paleodictyon* had a shield-like mound. The ventilation rate rapidly increased as the bottom current velocity increased. In contrast, the rate also increased with the height of the shield-like mounds, whereas it once dropped after the minor peak at 4 mm in height, which corresponds to the value measured in the modern specimens. This coincidence may imply that the height of the mound observed in modern specimens resulted from the optimization in balancing between the efficiency of ventilation and physical stability against erosion. Full exchange of water in the mesh structure by ventilation took less than a few minutes at this mound height, which is presumably sufficient for the ability of *Paleodictyon* producers.**

Keywords: **FLOW-3D, ichnology, paleoecology, passive ventilation, trace fossil**

Introduction

Paleodictyon is a common trace fossil found in deep-marine turbidite successions (Seilacher, 1967). This ichnogenus is characterized by a convex relief consisting of a regular hexagonal network preserved on the base of turbidite sandstone beds (Uchman, 1995, 2003; Cummings and Hodgson, 2011). It is interpreted that *Paleodictyon* is preserved as a cast of the burrows below the seafloor by the deposition of turbidites (Seilacher, 1977). In some specimens of *Paleodictyon*, a "nodose pattern" is observable as overprints on the hexagonal mesh structure (Seilacher, 1977). This is considered as evidence for the presence of the vertical tubes or tunnels open to the seafloor from the mesh structure, a few millimeters below the sediment-water interface (Seilacher, 1977, 2007). Specimens that have "nodose patterns" have been classified as *Paleodictyon nodosum* or *Paleodictyon tripatens* (Seilacher, 1977).

Numerous structures similar to *Paleodictyon nodosum* have been observed on the present deep seafloor. They are identified from the mid-Atlantic ridge (Rona and Merrill, 1978; Rona *et al.*, 2009), the South Atlantic (Ekdale, 1980), off New Caledonia (Gaillard, 1991), the eastern margin of Australia (Przeslawski *et al.*, 2012), and the eastern equatorial Pacific (Durden *et al.*, 2017). The morphology of the modern *Paleodictyon* is well described by Rona *et al.* (2009). In their survey, the modern specimens were observed as the arrangements of small dark-colored dots on the seafloor, which were the openings of the vertical tubes or tunnels (vertical shafts; Rona *et al.*, 2009). The diameter of the openings was less than 1 mm, and the openings of the vertical shafts were arranged in a hexagon 2–7.5 cm in diameter. The hexagonal mesh structure underlies the arrangement of dots on the seafloor. Notably, the seafloor rises as much as 5 mm toward the central

part of the arrangement, and forming a shield-like mound (Seilacher, 2007; Rona *et al.*, 2009). Although some specimens of the modern *Paleodictyon* have been collected as push cores, no producer has been discovered in the burrows (Rona *et al.*, 2009). Several researchers consider that *Paleodictyon* is a trace fossil produced by small endobenthic animals, which is interpreted as a trap for suspended food, a form for growing bacteria or fungi, or a foraging path (Seilacher, 1977; Uchman, 1995; Monaco, 2008; Lehane and Ekdale, 2013). In contrast, there are also arguments that *Paleodictyon* is an impression of a compressed hexactinellid sponge (Rona and Merrill, 1978; Ehrlich, 2019) or xenophyophores, large agglutinating protozoans (Swinbanks, 1982; Levin, 1994; Rona *et al.*, 2009).

In addition to the uncertainty of their producers, the functional morphology of the *Paleodictyon* burrow system is unknown. It was proposed that this unique morphology of *Paleodictyon* is a ventilation system that supplies oxygenated water and organic matter from bottom water to the mesh structure as a "passive ventilation" hypothesis (Seilacher, 1977, 2007). When the bottom current flows above the shield-like mound, a pressure difference occurs between the top and bottom of the mound owing to the velocity difference. Seawater in the mesh flows out through the low-pressure vertical shaft on the top of the mound, and bottom water flows into the mesh through high-pressure openings in the marginal area. This hypothesis was primarily proposed as a function for the bacterial farming in the burrow system (Seilacher, 1977). As mentioned above, there are several proposed origins of *Paleodictyon*. If *Paleodictyon* is the impression of hexactinellid sponge, they do not require the ventilation of water inside the mesh structure. In contrast, in addition to bacterial farming, this ventilating function is useful for the organism inside the structure in the cases of interpretation as food trapping or a foraminiferal test.

The "passive ventilation" hypothesis was tentatively confirmed by a flume experiment using a simplified plexiglas model and ink-stained water (Rona *et al.*, 2009). Observations showed that the ink-stained water was automatically drawn into the model from the margin and sucked out from the center. However, the hydraulic conditions or the setting of the experiment were not described quantitatively in their study. This is probably because of the technical difficulty in measuring the hydraulic conditions inside the mesh structure in physical flume experiments due to the complex morphology and small-scale tubes of *Paleodictyon*. Therefore, the ventilation hypothesis has not yet been adequately verified, and there are no quantitative data on ventilation.

This study examines the effects of *Paleodictyon*'s morphology on ventilation between bottom water and the mesh structure. To resolve the difficulty of measuring hydraulic conditions within a burrow system, three-dimensional numerical models of *Paleodictyon* with vertical shafts and a shield-like mound were constructed. Fluid simulations were then conducted to reconstruct the detailed hydraulic conditions in tunnels of *Paleodictyon* and the surrounding bottom water. The purpose of this study is to test the "passive ventilation" hypothesis for the functional morphology of *Paleodictyon*. Furthermore, quantitative data on the ventilation of the burrow system may provide information on the mode of life of their producers.

Numerical model

Governing equations

The fluid simulations were conducted using FLOW-3D (Flow Science, Inc.). In this study, the Reynolds-averaged Navier–Stokes (RANS) equations were numerically solved with the renormalization-group k-ε model for turbulence closure. The RANS are described by the following four equations representing conservation of mass (Eq. 1) and momentum (Eq. 2):

$$\frac{\partial}{\partial x}(uA_x)+\frac{\partial}{\partial y}(vA_y)+\frac{\partial}{\partial z}(wA_z)=0, \tag{1}$$

$$\begin{aligned}
&\frac{\partial u}{\partial t}+\frac{1}{V_F}\left(uA_x\frac{\partial u}{\partial x}+vA_y\frac{\partial u}{\partial y}+wA_z\frac{\partial u}{\partial z}\right)=-\frac{1}{\rho}\frac{\partial p}{\partial x}+G_x+f_x,\\
&\frac{\partial v}{\partial t}+\frac{1}{V_F}\left(uA_x\frac{\partial v}{\partial x}+vA_y\frac{\partial v}{\partial y}+wA_z\frac{\partial v}{\partial z}\right)=-\frac{1}{\rho}\frac{\partial p}{\partial y}+G_y+f_y,\\
&\frac{\partial w}{\partial t}+\frac{1}{V_F}\left(uA_x\frac{\partial w}{\partial x}+vA_y\frac{\partial w}{\partial y}+wA_z\frac{\partial w}{\partial z}\right)=-\frac{1}{\rho}\frac{\partial p}{\partial z}+G_z+f_z,
\end{aligned} \tag{2}$$

where u, v, and w denote the velocity components in the coordinates x, y, and z, respectively; ρ and p are expressed by the fluid density and the fluid pressure, respectively; G_x, G_y, and G_z exhibit the body accelerations in each coordinate direction; and f_x, f_y, and f_z denote the viscous accelerations in each coordinate direction. In this model, the fractional area-volume obstacle representation (FAVOR) method was employed for processing the flow near the surface of arbitrary geometry of objects in Cartesian coordinates. A_x, A_y, and A_z are the fractional area open to flow in each coordinate direction, and V_F is the volume fraction of fluid.

The renormalization-group (RNG) k-ε model (Yakhot *et al.*, 1992) was employed as the turbulence model in this study. In the RNG k-ε model, eddy viscosity μ is given by

$$\mu=\rho C_\mu\frac{k^2}{\varepsilon} \tag{3}$$

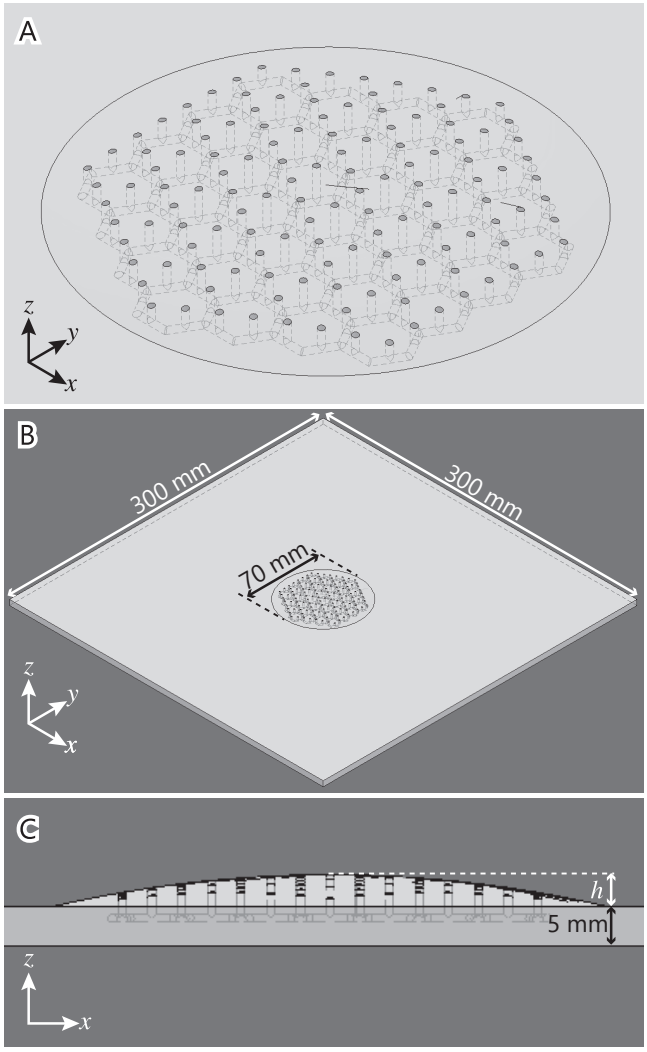

Figure 1. Example of the 3D model of *Paleodictyon* and its dimensions. **A,** Close up view of the hexagonal mesh, vertical shafts, and shield-like mound. The tunnels are 1 mm in diameter. The diagonal line of each hexagon is 10 mm in length. **B,** Complete view of the 3D model embedded in the board, compared to the seafloor. **C,** Lateral view of the 3D model around the shield-like mound.

where C_μ is an empirical coefficient, and k and ε are the turbulence kinetic energy and dissipation, respectively. In FLOW-3D, the conservation of k and ε are computed as follows:

$$\frac{\partial k_T}{\partial t}+\frac{1}{V_F}\left(uA_x\frac{\partial k_T}{\partial x}+vA_y\frac{\partial k_T}{\partial y}+wA_z\frac{\partial k_T}{\partial z}\right)=P_T+G_T+D_{k_T}-\varepsilon_T, \quad (4)$$

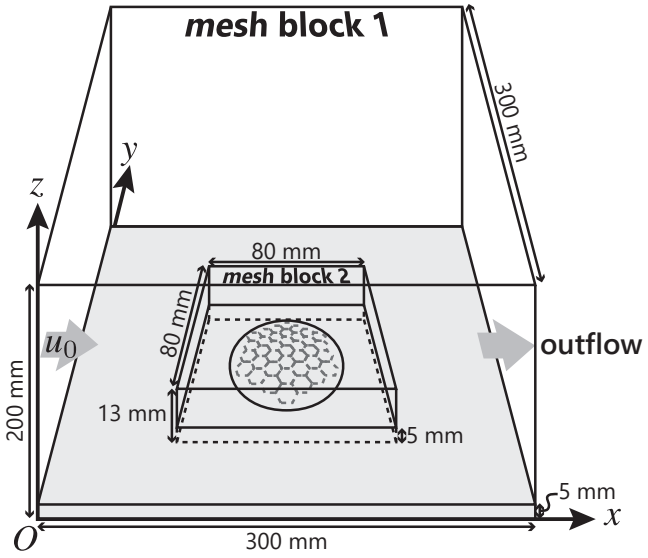

Figure 2. Calculation domain and mesh grids using in the fluid simulations. u_0: initial velocity of bottom current.

$$\frac{\partial \varepsilon_T}{\partial t}+\frac{1}{V_F}\left(uA_x\frac{\partial \varepsilon_T}{\partial x}+vA_y\frac{\partial \varepsilon_T}{\partial y}+wA_z\frac{\partial \varepsilon_T}{\partial z}\right)=\frac{C_1\varepsilon_T}{k_T}(P_T+C_3G_T)+D_{\varepsilon_T}-C_2\frac{{\varepsilon_T}^2}{k_T}, \quad (5)$$

where P_T denotes the turbulent kinetic energy production and G_T is expressed by the buoyancy production term. The diffusion and dissipation of turbulent kinetic energy are denoted by D_{k_T} and D_{ε_T}, respectively. C_1, C_2, and C_3 exhibit dimensionless parameters with default values of 1.44, 1.92, and 0.2, respectively (Flow Science, Inc., 2012).

3D model of *Paleodictyon*

The 3D morphology of *Paleodictyon* (Figure 1) was constructed using the 3D CAD software Autodesk Inventor 2017 (Autodesk, Inc.). The internal diameter of the hexagonal tunnels and vertical shafts was set to 1 mm. The length of the diagonal line of the hexagons was set to 10 mm. The number of hexagons in the mesh structure was 37. On the midpoint of each side of the hexagon, the vertical shaft was arranged to connect the mesh structure to the seafloor (Figure 1A). Topography of the seafloor above the burrows portrayed the shield-like mound, rendered as a solid arc of 70 mm revolution in chord length. In this study, to examine the influence of the height of the mound, nine models were produced by changing the arc of the mounds from 0 to 8 mm at 1 mm intervals (Figure 1C). The hexagonal mesh and vertical shafts were embed-

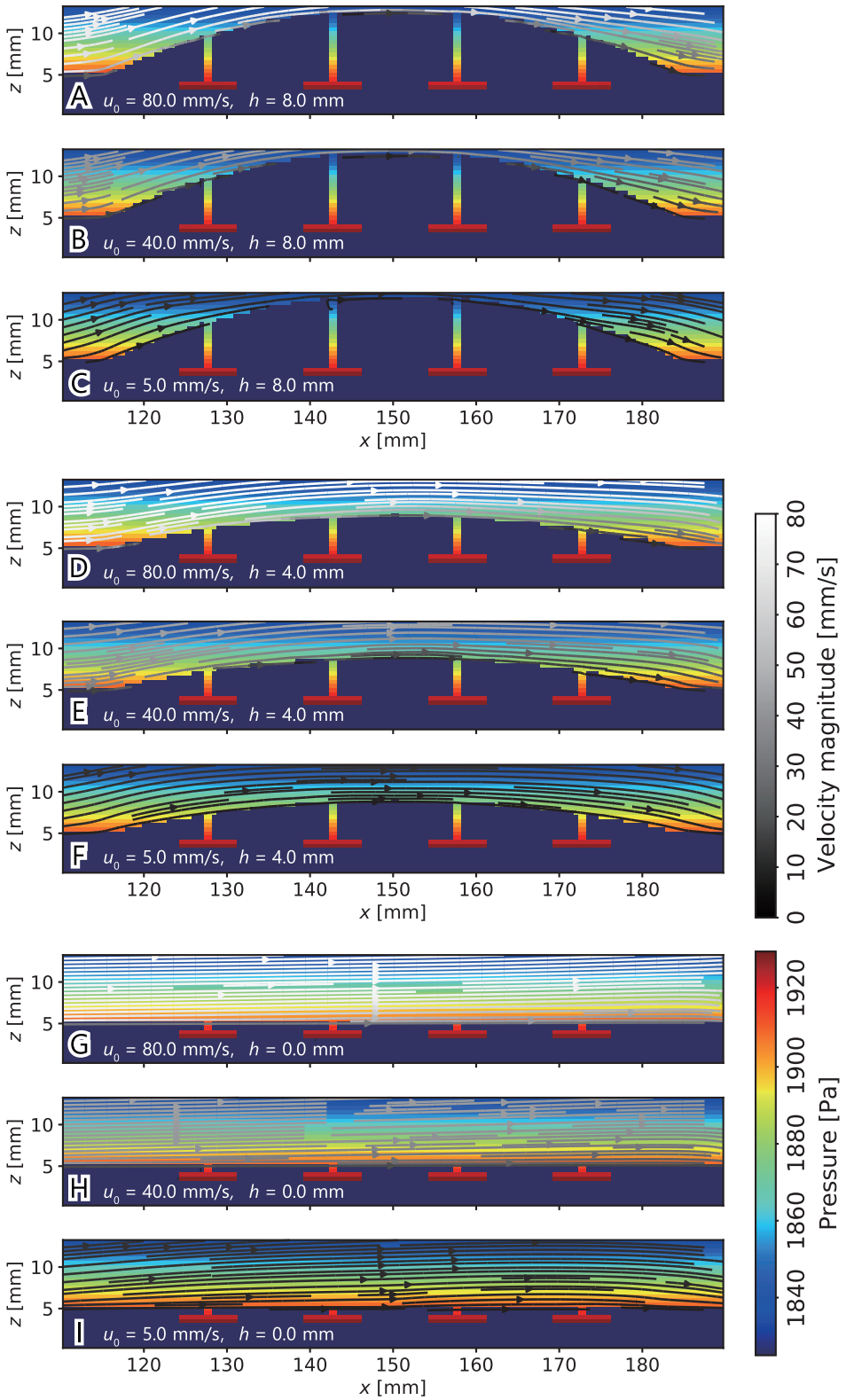

Figure 3. Pressure field and flow direction in each condition at t = 20 s. Each diagram represents the cross-sectional view at y = 150 mm. Colors show the pressure and velocity magnitude of the stream lines. **A,** u_0 = 80.0 mm/s and h = 8.0 mm; **B,** u_0 = 40.0 mm/s and h = 8.0 mm; **C,** u_0 = 5.0 mm/s and h = 8.0 mm; **D,** u_0 = 80.0 mm/s and h = 4.0 mm; **E,** u_0 = 40.0 mm/s and h = 4.0 mm; **F,** u_0 = 5.0 mm/s and h = 4.0 mm; **G,** u_0 = 80.0 mm/s and h = 0.0 mm; **H,** u_0 = 40.0 mm/s and h = 0.0 mm; **I,** u_0 = 5.0 mm/s and h = 0.0 mm.

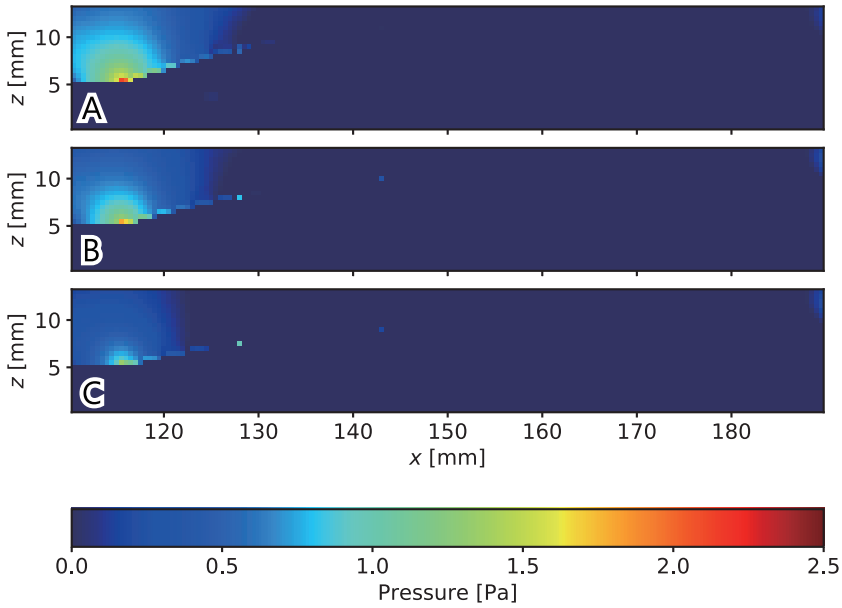

Figure 4. Cross-sectional view of the dynamic pressure fields at y = 150 mm. **A,** u_0 = 80.0 mm/s and h = 6.0 mm; **B,** u_0 = 80.0 mm/s and h = 5.0 mm; **C,** u_0 = 80.0 mm/s and h = 4.0 mm.

ded in a non-erodible solid object that was 300 × 300 × 5 mm (Figure 1B).

Calculation domain and mesh grids

The calculation domain was set to 300 × 300 × 200 mm for all experiments, and the 3D model of *Paleodictyon* was placed on the bottom of the flume. Two types of mesh blocks were set in the domain. Mesh block 1 covered the entire region of the calculation domain, and was 10 mm in grid spacing. Mesh block 2 covered an area of 80 × 80 × 13 mm around *Paleodictyon*, with 0.5 mm grid spacing to reproduce detailed flow dynamics near the burrow system (Figure 2). In this study, the streamwise direction was set parallel to the x-coordinates. The boundary conditions of the flow velocity at the upstream end (x = 0 mm) were varied from 5 to 80 mm/s. In the Atlantic Ocean, where modern *Paleodictyon* was observed, flow up to 80 mm/s was recorded 150 m above the seafloor (Rona *et al.*, 2009). Therefore, it is possible that the bottom current velocity near the sediment-water interface may be lower than this case, so the upper limit was set to 80 mm/s in this study. The numerical experiments in this study were conducted at nine different initial flow velocities u_0 (5 mm/s at the start, increasing from 10 to 80 mm/s at 10 mm/s intervals). The flow duration was 20 s for each experiment. At the upstream end (x = 0 mm), the boundary conditions involved a constant flow velocity, which also varied from 5 mm/s at the beginning, and 10–80 mm/s, at 10 mm/s intervals for each experiment. For lateral sides of the calculation domains, periodic boundary conditions were applied (y = 0, 300 mm). Outflow boundary conditions (Flow Science, Inc., 2012) were involved at the downstream end (x = 300 mm). In all experiments, the calculation domain was entirely filled with water (20°C in temperature), and the wall boundary conditions were applied to the upper boundary (z = 200 mm).

Evaluation of the ventilation rate in burrows

The ventilation rate in a burrow was estimated as the volumetric discharge of outflow from the hexagonal mesh structure through the vertical shafts. The z-component of velocity in each vertical shaft was measured at an elevation of 2.5 mm above the mesh structure. Then, the ventilation rate Q_v was computed as

$$Q_v = \sum_i^n W_i A \quad \begin{cases} w_i > 0, & W_i = w_i \\ \text{otherwise}, & W_i = 0 \end{cases} \qquad (6)$$

where n denotes the number of vertical shafts, w_i is expressed by the averaged z-directional velocity for the i-th shaft, and A is the cross-sectional area of a shaft (A = 0.785 mm^2 in this study).

Results

Flow velocity and pressure field around the mound

In all cases, the bottom current flowed parallel to the geometry of the seafloor, and flow separation behind the

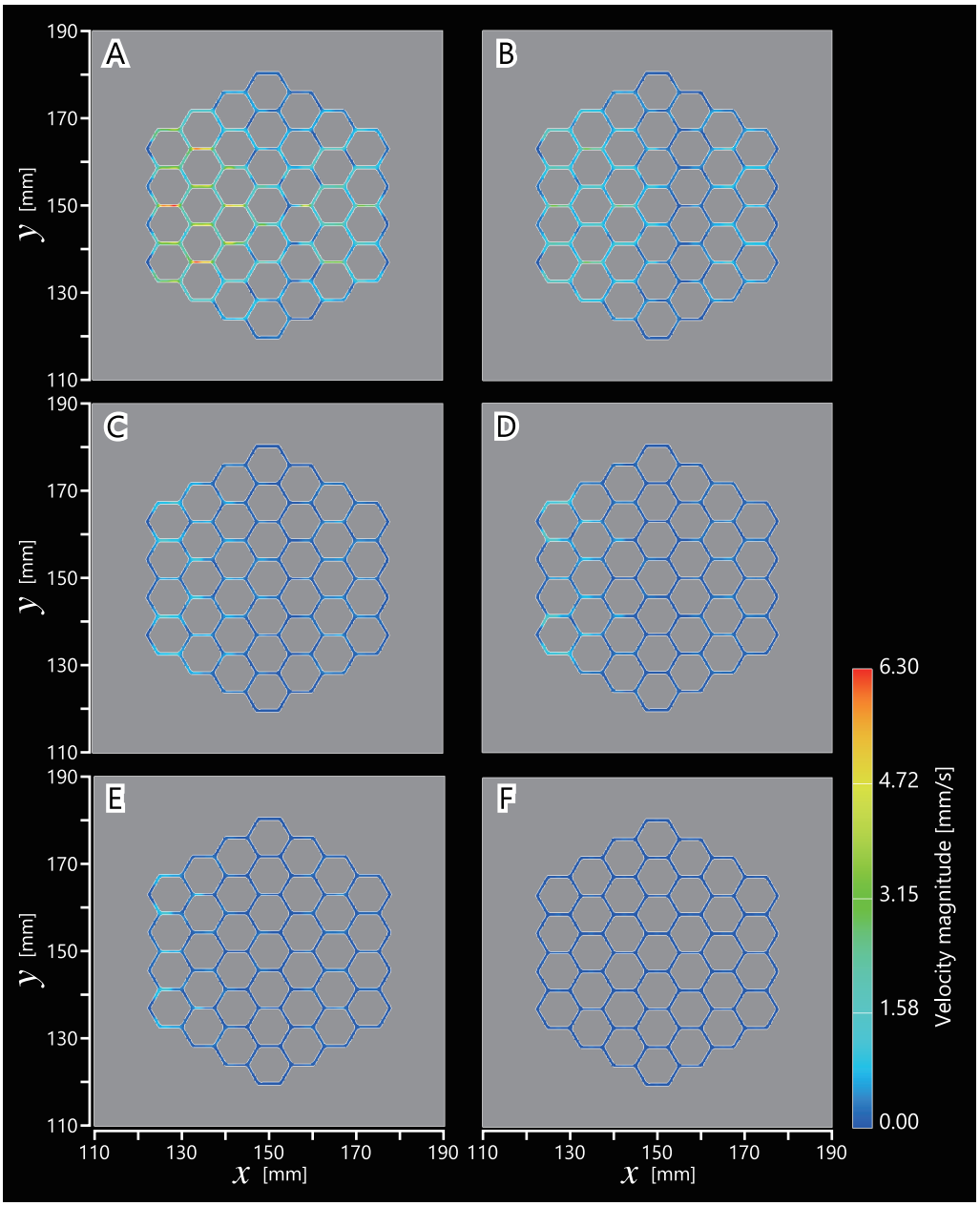

Figure 5. Change of velocity magnitude in the mesh structure at z = 3.0 mm depending on height of the shield-like mound h. The initial bottom current velocity u_0 was 80.0 mm/s in all cases. **A**, h = 8.0 mm; **B**, h = 6.0 mm; **C**, h = 5.0 mm; **D**, h = 4.0 mm; **E**, h = 3.0 mm; **F**, h = 0.0 mm (no shield-like mound).

mound was not observable (Figure 3). The velocity difference between the marginal and center areas of the mounds ranged from 3.7 to 70.0 mm/s.

The pressure in the calculation domain around the burrow system ranged from 1,829 to 1,929 Pa (Figure 3). The pressure tended to be higher with increasing bottom current velocity. The difference in water pressure between the center and marginal areas of the shield-like mound ranged from 9.8 to 79.2 Pa, depending on the velocity of the bottom currents or height of the mound (Figure 3). A dynamic pressure of up to 2.5 Pa was observed on the upstream side of the mounds (Figure 4). In the case of flat topography, there was no pressure difference between the center and marginal areas of the burrow system or the velocity (Figure 3G–I).

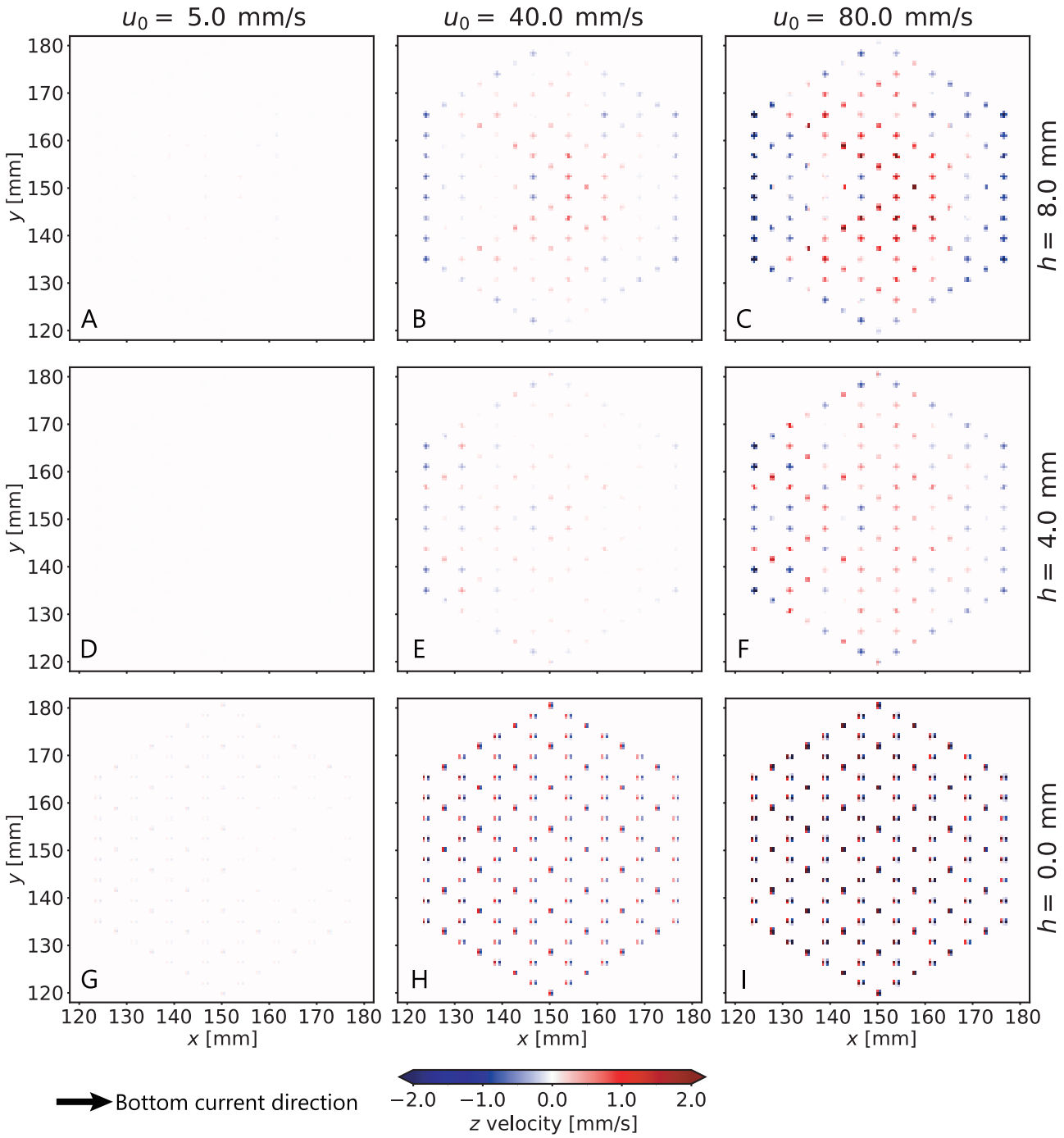

Figure 6. Examples of distribution of *z*-directional velocity in the vertical shafts at z = 4.5 mm and t = 20 s. The shield-like mound becomes higher on the upper columns and the bottom current velocity increases rightward in rows. The colors of each point show the *z*-directional velocity: the red points indicate outflow from vertical shafts and the blue points show inflow to the hexagonal mesh structure. Bottom current direction was from left to right. **A–C,** h = 8 mm; **D–F,** h = 4 mm; **G–I,** h = 0 mm (no shield-like mound).

Flow velocity field inside the burrow systems

Flow velocity up to 6.3 mm/s was observed inside the mesh structure in the experiments with the shield-like mounds (Figure 5). The velocity magnitude increased depending on the bottom current velocity, and tended to be higher in the upstream region of the burrow than in the downstream region (Figure 5A–E). Conversely, in the case of experiments with flat topography, almost no flow

discharge was observed in the mesh structure (Figure 5F).

Vertical flows of ventilated water inside the mesh structure were observed in most cases, while the flow velocity depended on both of the bottom current and height of the mound-like topography. The flow velocities at time t = 20 s ranged from −6.9 to 5.0 mm/s. Although the velocity field inside the vertical shafts did not change over time, the flow velocity largely varied depending on the location in the mound. Outlet and inlet flows were observed in the central and marginal areas of the mound, respectively. At u_0 = 8.0 mm/s and h = 8.0 mm, the vertical flow velocity tended to be positive, and was up to 5.0 mm/s in the central area. In contrast, velocity in the marginal area was negative, at least −4.0 mm/s (Figure 6C). Furthermore, the location of the outlet coincides to that of low-pressure region (Figures 3, 6). The velocity of the inlet and outlet flows depended on both the initial bottom current velocity (u_0) and the height of the shield-like mound (h) (Figure 6). In the case of a low u_0 (5–30 mm/s), the maximum velocity in the vertical shafts was lower than 1 mm/s. In contrast, it reached 5 mm/s in the higher u_0 cases (40–80 mm/s), which is 10 to 100 times higher than that of the cases with a lower flow velocity. In addition, the absolute value of the flow velocity in the vertical shafts tended to increase with an increase in h (Figure 6).

In the case of experiments with flat topography, the circulating flow was developed in a vertical shaft, in which the opposite directional flows were observed in a single vertical shaft (Figure 6G–I). In this case, the net flux of the outlet or inlet flow in a vertical shaft was approximately zero; therefore, this circulating flow inside the vertical shafts did not contribute to the ventilation of the water in the mesh tunnels.

Ventilation rate

The ventilation rate Q_V was calculated for the vertical shafts without circulation flow. The time series of Q_V showed that they achieved steady state in a few seconds after the simulation started (Figure 7). Therefore, this study calculated Q_V at t = 20 s for each condition.

The general trend is that Q_V increased with increasing u_0 and h (Figures 8, 9). For instance, when u_0 increased by 1 mm/s at any given h, Q_V becomes 1.4–5.0 times larger (Figure 9B). In contrast, at a constant u_0, Q_V increases approximately 1.2–2.0 times when h increases by 1 mm (Figure 9A). The largest Q_V (= 46.18 mm^3/s) was recorded at u_0 = 80 mm/s and h = 8 mm. However, changes in Q_V associated with increasing h are not a monotonic increase. A higher h leads to a higher Q_V between h = 0 to 4 mm, and then Q_V decreases once at h = 5 mm. In the range of h = 6–8 mm, Q_V increases again with increasing h (Figures 8, 9A). In the cases of no shield-like mound, Q_V was 0 because the circulation flow occurred.

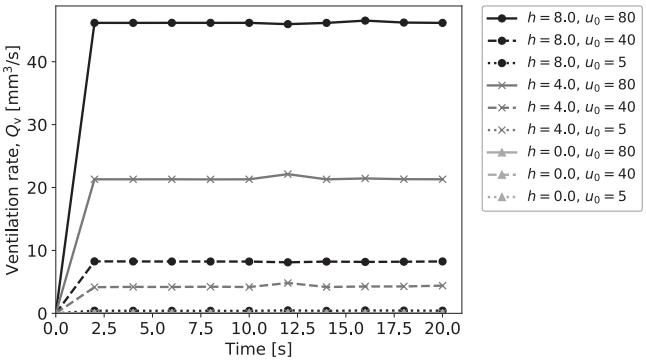

Figure 7. Examples of time series of Q_V.

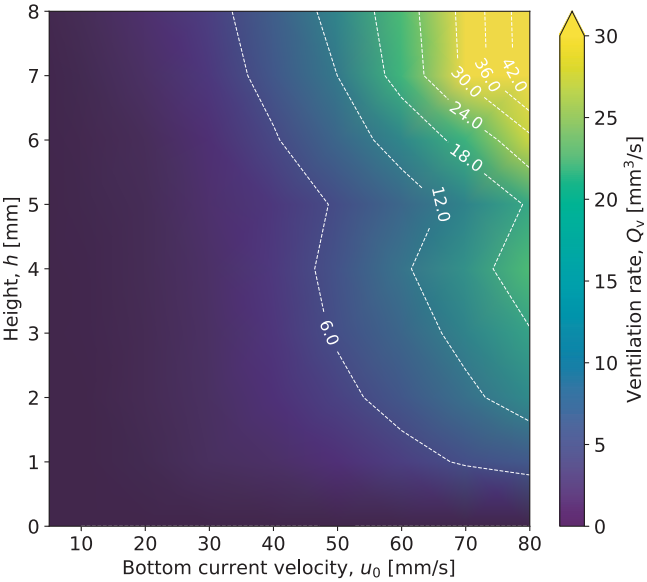

Figure 8. Distribution of ventilation rate Q_V on the u_0–h plane.

Shear velocity

The maximum shear velocity on the bottom surface ranged from 1.78×10^{-3} to 1.22×10^{-2} m/s in numerical experiments of this study. In general trend, the shear velocity on the upstream side of the shield-like mound was higher than that on the downstream side (Figure 10). The maximum shear velocity increased associated with increase of the mound height (Figure 10). The highest shear velocity (1.22×10^{-2}) was observed on the top of the mound in the case of h = 8 mm and u_0 = 80 mm/s.

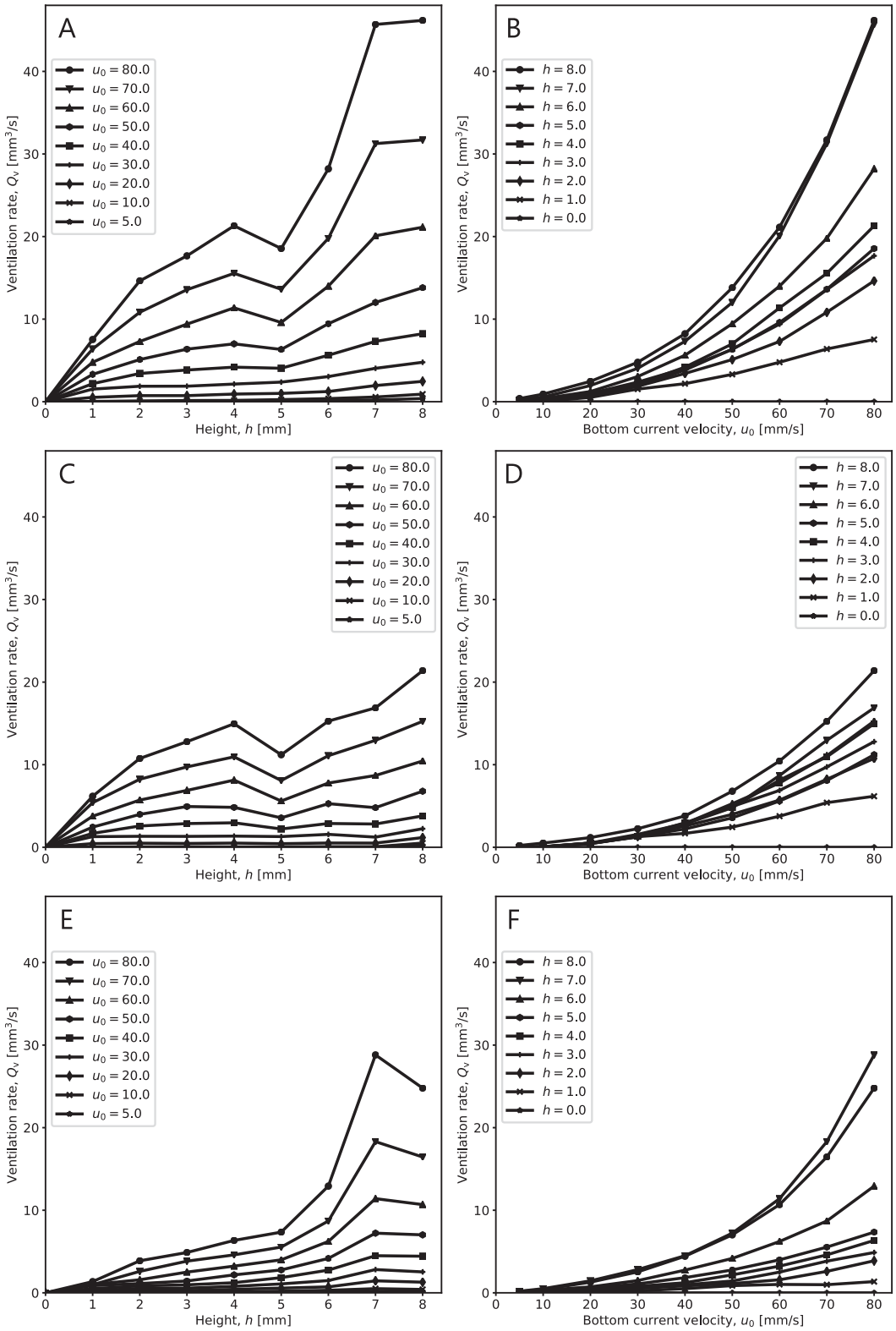

Figure 9. Fluctuation of ventilation rate Q_v associated with increase in height of shield-like mound h (left column) and bottom current velocity u_0 (right column). **A, B,** Ventilation rates from all the vertical shafts; **C, D,** Ventilation rates from the vertical shafts on the upstream side ($x \leq 150$ mm); **E, F,** Ventilation rates from the vertical shafts on the downstream side ($x > 150$ mm).

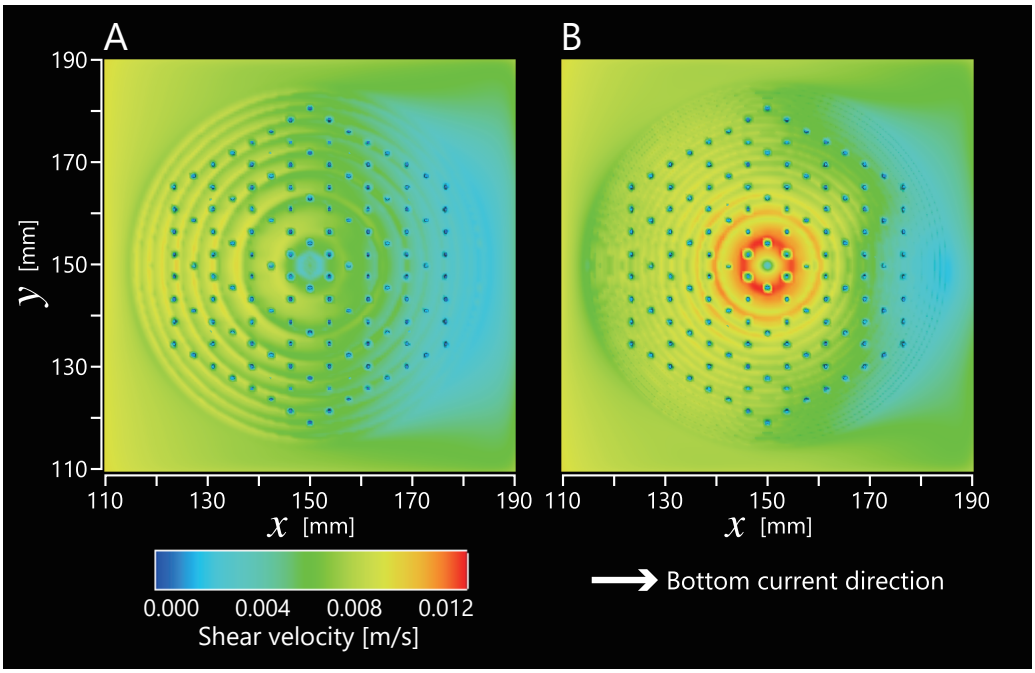

Figure 10. Shear velocity field on the shield-like mounds at u_0 = 80 mm/s and t = 20 s. **A,** h = 4 mm; **B,** h = 8 mm.

Discussion

The results of fluid simulations suggest that the ventilation of the water between the bottom water and the mesh structure occurs when the shield-like mound exists on the top of the burrow system. These results support the hypothesis that the shield-like mound and vertical shafts are useful for ventilation. In the cases where *Paleodictyon* has no shield-like mound, ventilation between the bottom water and the mesh structure did not occur (Figures 8, 9). The pressure fields suggest that the ventilation was mainly caused by the pressure difference that resulted from the dynamic pressure of the bottom current at the slope of the mound (Figure 4).

The height of the shield-like mound strongly affects the ventilation rate, which increases as the mound height increases, except for the region from 4 to 5 mm. The decrease in the ventilation rate Q_V at h = 5 mm might be a result of interference of the flow within the mesh structure. In the experiments with 0–4 mm mound elevation, the internal flow in the upstream region of the mound is much larger than that in the downstream (Figure 5). The ventilation system was active mainly in the upstream region as the result. In contrast, the internal flow in the downstream region became active at a mound elevation above 4 mm. The decline of the ventilation rate coincides with this activation of the downstream region of the burrow system (Figures 4, 9C, E). This implies that it became transiently difficult for the bottom water to find the efficient flow paths in the mesh structure from the upstream side, due to the increase in inflow from the downstream side.

The height of the shield-like mound observed in modern *Paleodictyon* specimens can be interpreted as a consequence of balancing the high ventilation rate and the physical stability of the mounds. Modern *Paleodictyon* specimens collected by Rona *et al.* (2009) had shield-like mounds that were up to 5 mm in height (Rona *et al.*, 2009), although the original height might have been slightly lower because the mounds might be deformed and emphasized by the process of core sampling. If the *Paleodictyon* producers formed a shield-like mound in order to gain high ventilation efficiency, it is preferable for them to build a higher mound. However, high shield-mounds are physically unstable because the higher bed shear stress causes erosion on the top of the mounds.

Here, the stability of the mound against erosion is discussed from the results of numerical calculations. The critical shear stress τ_c^* for initiation of motion of fine-grained, noncohesive sediments can be estimated as following empirical equation (Garcia, 2008):

$$\tau_c^* = 0.135 R_{ep}^{-0.261} \quad (7)$$

where R_{ep} is the particle Reynolds number which is given by

$$R_{ep} = \frac{\sqrt{gRD}D}{v} \quad (8)$$

where v is the kinetic viscosity of water which is 10^{-6} m^2/s at 20°C, g is the gravitational acceleration, R denotes the submerged specific gravity of the sediment (1.65), and D is expressed by the sediment particle diameter. The Shields number τ^* can be calculated by

$$\tau^* = \frac{u_*^2}{gRD} \quad (9)$$

where u_* is the shear velocity. The *Paleodictyon* mound reported by Rona *et al*. (2009) was composed of lutite, *i.e.* silt or clay particles. When the sediment particle diameter D is set to the maximum size of silt particle (= 0.063 mm), the critical shear stress τ_c^* is calculated as 0.112. In the case of h = 4 mm and u_0 = 80 mm/s, the maximum shear velocity on the shield-like mound was 1.05×10^{-2} (Figure 10), so that τ^* was 0.108, which is less than the critical shear stress τ_c^*. This implies that no sediment motion occurs at this condition. In contrast, τ^* = 0.147 was calculated using the maximum shear velocity 1.22×10^{-2} at the condition h = 8 mm and u_0 = 80 mm/s (Figure 10). This value is larger than the critical shear stress, suggesting the possibility that sediment transport and resulting erosion on the top of the mounds higher than 4 mm. Furthermore, even if the shield-like mound was formed above 7 mm, the ventilation rate did not change significantly (Figure 9A). Taking these into consideration, the height of modern shield-like mounds is reasonable for the *Paleodictyon* producers because of the balance between a relatively high ventilation rate and physical stability.

The results of the numerical experiments indicate that the water in the mesh structure can be fully ventilated for less than several minutes. In the case of h = 4 mm and u_0 = 80 mm/s, the ventilation rate is calculated as 21.3 mm^3/s (Figure 9), and the volume of the mesh structure in the 3D models was approximately 518.1 mm^3. Therefore, approximately 4% of water in the mesh structure can be exchanged each second. This indicates that a 25 s duration of 80 mm/s bottom current can fully ventilate the water in the mesh structure. Even if the bottom current velocity is 40 mm/s, it takes only approximately 2 min for complete ventilation. Note that the values of ventilation rate may be different in the natural cases in comparison to that from the calculation because of low temperature in actual deep-marine although the calculations reflect some tendencies. Since the water temperature at the time of *Paleodictyon* formation is unknown, the calculations in this study tentatively set the water temperature to 20°C. However, if we assume that water temperature is 4°C, the kinetic viscosity becomes 1.6×10^{-6} m^2/s, which is approximately 1.6 times as high as that at 20°C. Therefore, if the Reynolds similarity law holds, the same phenomenon as in the present numerical experiments occurs at this water temperature when the flow velocity is 1.6 times as high as the value set in this study.

The optimized morphology of the burrow system of *Paleodictyon* to ventilate water inside the mesh structure implies the ecology of the producer. Ventilation may be useful for respiration and/or feeding of the producer that requires the exchange of water in the burrow system. Although the *Paleodictyon*-producing animal remains unknown, *Paleodictyon* has been suggested as a biogenic sedimentary structure by a single or colonial burrower (Wetzel, 2000), farming trace (Seilacher, 1977; Monaco, 2008), or an impression of an infaunal xenophyphore, which is a large agglutinating protist (Swinbanks, 1982; Tendal *et al.*, 1982; Levin, 1994). Levin (1994) implied that vertical shafts in the *Paleodictyon* burrow system can be used as the outlets of pseudopodia, or the vents to oxygenate the body of the xenophyphore. The results of our numerical experiments support the latter possibility. In any case, further investigation to determine the producer of *Paleodictyon* will provide more insights into the function of the morphology of this burrow system.

Conclusions

Fluid simulations indicate that the vertical shafts within the mound-like shape of the *Paleodictyon* burrow system serves to ventilate the water inside its burrow tubes through a mesh structure. This passive ventilation with bottom currents requires a shield-like mound on the top of the burrow system, which causes a pressure difference between the top and marginal areas of the mound. The pressure difference was caused by the dynamic pressure on the upstream side of the mound. In the case of no shield-like mound, seawater circulated only in the vertical shaft and did not exchange beyond the sediment-water interface. As the height of the mound increases, the value of the ventilation rate also increases and reaches a maximum at a height h = 4 mm. After this local peak, the ventilation rate was lowered, in the range of 4–6 mm, then the rate increased again with the height of the mound. Thus, larger values of mound height result in higher rates of ventilation. However, physical instability also occurs because of high bed shear stress when the mound becomes too high. Indeed, the actual height of the mound of modern *Paleodictyon* matched the height corresponding to the local peak of the ventilation rate, implying that it can be a balanced condition between water exchange and the stability of the burrow system. Even though the *Paleodictyon* producers still remain unknown, this optimized morphology for the function to ventilate the water

in burrow tubes may be a key in understanding their ecology.

Acknowledgments

Dr. Alfred Uchman and two anonymous reviewers critically read the manuscript and made helpful suggestions. This study was supported by the Sediment Dynamics Research Consortium (sponsored by INPEX, JOGMEC, JX Nippon Oil & Gas Exploration Corporation and JAPEX) for the funding. All of these contributions are gratefully acknowledged.

References

Cummings, J. P. and Hodgson, D. M., 2011: Assessing controls on the distribution of ichnotaxa in submarine fan environments, the Basque Basin, Northern Spain. *Sedimentary Geology*, vol. 239, p. 162–187.

Durden, J. M., Simon-Lledo, E., Gooday, A. J. and Jones, D. O., 2017: Abundance and morphology of *Paleodictyon nodosum*, observed at the Clarion-Clipperton Zone. *Marine Biodiversity*, vol. 47, p. 265–269.

Ehrlich, H., 2019: *Paleodictyon*—Enigmatic honeycomb structure. *In*, Ehrlich, H. *ed.*, *Marine Biological Materials of Invertebrate Origin*, p. 81–85. Springer, Cham.

Ekdale, A., 1980: Graphoglyptid burrows in modern deep-sea sediment. *Science*, vol. 207, p. 304–306.

Flow Science, Inc., 2012: *FLOW-3D Documentation, Release 10.1.0*, 819 p. Flow Science, Inc., Santa Fe.

Gaillard, C., 1991: Recent organism traces and ichnofacies on the deep-sea floor off New Caledonia, southwestern Pacific. *Palaios*, vol. 6, p. 302–315.

Garcia, M., 2008: Sediment transport and morphodynamics. *In*, Garcia, M. *ed.*, *Sedimentation Engineering: Processes, Measurements, Modeling, and Practice*, p. 21–163. American Society of Civil Engineers, Virginia.

Lehane, J. R. and Ekdale, A., 2013: Pitfalls, traps, and webs in ichnology: traces and trace fossils of an understudied behavioral strategy. *Palaeogeography*, *Palaeoclimatology*, *Palaeoecology*, vol. 375, p. 59–69.

Levin, L. A., 1994: Paleoecology and ecology of xenophyophores. *Palaios*, vol. 9, p. 32–41.

Monaco, P., 2008: Taphonomic features of *Paleodictyon* and other graphoglyptid trace fossils in Oligo–Miocene thin-bedded turbidites, northern Apennines, Italy. *Palaios*, vol. 23, p. 667–682.

Przeslawski, R., Dundas, K., Radke, L. and Anderson, T. J., 2012: Deep-sea Lebensspuren of the Australian continental margins. *Deep Sea Research Part I: Oceanographic Research Papers*, vol. 65, p. 26–35.

Rona, P. A. and Merrill, G. F., 1978: A benthic invertebrate from the Mid-Atlantic Ridge. *Bulletin of Marine Science*, vol. 28, p. 371–375.

Rona, P. A., Seilacher, A., de Vargas, C., Gooday, A. J., Bernhard, J. M., Bowser, S., Vetriani, C., Wirsen, C. O., Mullineaux, L., Sherrell, R., Grassle, J. F., Low, S. and Lutz, R. A., 2009: *Paleodictyon nodosum*: a living fossil on the deep-sea floor. *Deep Sea Research Part II: Topical Studies in Oceanography*, vol. 56, p. 1700–1712.

Seilacher, A., 1967: Bathymetry of trace fossils. *Marine Geology*, vol. 5, p. 413–428.

Seilacher, A., 1977: Pattern analysis of *Paleodictyon* and related trace fossils. *In*, Crimes, T. P. and Harper, J. C. *eds.*, *Trace Fossils 2: Geological Journal*, *Special Issue*, vol. 9, p. 289–334.

Seilacher, A., 2007: *Trace Fossil Analysis*, 226 p. Springer, Berlin and Heidelberg.

Swinbanks, D., 1982: *Paleodictyon*: the traces of infaunal xenophyophores? *Science*, vol. 218, p. 47–49.

Tendal, O., Swinbanks, D. and Shirayama, Y., 1982: A new infaunal xenophyophore (Xenophyophorea, Protozoa) with notes on its ecology and possible trace fossil analogs. *Oceanologica Acta*, vol. 5, p. 325–329.

Uchman, A., 1995: Taxonomy and palaeoecology of flysch trace fossils: The Marnoso-arenacea Formation and associated facies (Miocene, Northern Apennines, Italy). *Beringeria*, vol. 15, p. 3–115.

Uchman, A., 2003: Trends in diversity, frequency and complexity of graphoglyptid trace fossils: evolutionary and palaeoenvironmental aspects. *Palaeogeography*, *Palaeoclimatology*, *Palaeoecology*, vol. 192, p. 123–142.

Wetzel, A., 2000: Giant *Paleodictyon* in Eocene flysch. *Palaeogeography*, *Palaeoclimatology*, *Palaeoecology*, vol. 160, p. 171–178.

Yakhot, V., Orszag, S., Thangam, S., Gatski, T. and Speziale, C., 1992: Development of turbulence models for shear flows by a double expansion technique. *Physics of Fluids A: Fluid Dynamics*, vol. 4, p. 1510–1520.

Author contributions

K. K. initiated the study, conducted the numerical simulations, and analyzed and interpreted data. H. N. interpreted data and revised the manuscripts.